

Enantioselective cellular uptake of chiral semiconductor nanocrystals

This content has been downloaded from IOPscience. Please scroll down to see the full text.

2016 Nanotechnology 27 075102

(<http://iopscience.iop.org/0957-4484/27/7/075102>)

View [the table of contents for this issue](#), or go to the [journal homepage](#) for more

Download details:

IP Address: 144.122.201.150

This content was downloaded on 20/01/2016 at 14:49

Please note that [terms and conditions apply](#).

Enantioselective cellular uptake of chiral semiconductor nanocrystals

I V Martynenko¹, V A Kuznetsova², I K Litvinov¹, A O Orlova¹, V G Maslov¹,
A V Fedorov¹, A Dubavik¹, F Purcell-Milton², Yu K Gun'ko^{1,2} and
A V Baranov¹

¹ITMO University, 49 Kronverksky pr., St. Petersburg, 197101, Russia

²School of Chemistry and CRANN, Trinity College Dublin, Dublin 2, Ireland

E-mail: a.o.orlova@gmail.com

Received 4 August 2015, revised 26 November 2015

Accepted for publication 7 December 2015

Published 19 January 2016



CrossMark

Abstract

The influence of the chirality of semiconductor nanocrystals, CdSe/ZnS quantum dots (QDs) capped with *L*- and *D*-cysteine, on the efficiency of their uptake by living Ehrlich Ascite carcinoma cells is studied by spectral- and time-resolved fluorescence microspectroscopy. We report an evident enantioselective process where cellular uptake of the *L*-Cys QDs is almost twice as effective as that of the *D*-Cys QDs. This finding paves the way for the creation of novel approaches to control the biological properties and behavior of nanomaterials in living cells.

Keywords: CdSe/ZnS quantum dots, chirality, FLIM, living cells

(Some figures may appear in colour only in the online journal)

1. Introduction

Chirality is a characteristic of the majority of biologically active molecules, and is responsible for their stereospecific interactions with the environment. Many properties such as cell penetration, enzymatic activity and toxicity are all strongly dependent on the chirality of substances [1].

The creation of man-made chiral inorganic structures constitutes an important developing area in contemporary chemistry and nanotechnology [2–4]. Producing nanostructures with chiral properties may lead to significant changes in their interactions with biomolecules and opens up new possibilities to obtain stereospecific interactions of nanostructures in a biological environment [5].

Semiconductor quantum dots (QDs) [6] are a distinct example of man-made inorganic nanoparticles that can be widely used in many fields of biological applications [7–11]. Recent studies have demonstrated induced chiroptical activity in QDs [12–15]. These chiral QDs can be produced by a range of different approaches, including the use of chiral molecules as stabilizers in colloidal synthesis of QDs [13, 14] or as capping ligands in post-synthesis phase transfer [16, 17].

It has been proposed that these chiral properties of QDs may influence their ability to interact with biomolecules and thereby modulate a range of vital processes in living cells. An

aspect of this has been demonstrated for glutathione-coated CdTe QDs [18] with cell toxicity associated in part to the chirality of the glutathione coating, with *D*-glutathione-capped CdTe QDs, the non-biologically active form of glutathione, showing lower cytotoxicity than *L*-glutathione-coated CdTe QDs.

Among others, the influence of QD chirality on their cellular uptake and therefore the dot concentration in a cell is of great importance. To undertake a meaningful comparative *in-vitro* study of the intracellular uptake of QDs of different chirality, it is essential to accurately determine their concentrations in the cells. Inductively coupled plasma mass spectrometry (ICP-MS) [19] appears to be the most reliable technique for determination of QD cell concentration through element concentration e.g., estimation of Cadmium and Zinc content in the case of CdSe/ZnS QDs. However, in the case of living cells, this technique meets some difficulties upon preparation of the samples for the ICP measurements. From this point of view, a fast, nondestructive, sensitive, and possessing high spatial resolution fluorescence (FL) microspectroscopy, both stationary and time-resolved, looks attractive enough. Fluorescence analysis can be applied for quantitative comparison of concentrations of different fluorophores in the cells under certain conditions though a simple comparison of absolute intensities cannot be considered as

convincing since the fluorescence signal of quantum dots incubated in complicated multicomponent ionic and biological media can depend on a variety of external environments [20, 21]. This comparison only carries meaning if the ratio of the fluorescence quantum yields of both QD enantiomers in the cell is the same as in the initial solutions and therefore displays an absence of enantioselective fluorescence quenching upon QD incorporation into the cells. This can be verified by comparison of the fluorescence decay times for the QD enantiomers in solutions and in the cells, which is achieved by fluorescent lifetime imaging microscopy (FLIM) [20, 22, 23].

In the present study, we have investigated the influence of the chirality of CdSe/ZnS core-shell quantum dots on their cellular uptake by *in vitro* comparative analysis of fluorescence properties of chiral QDs in living Ehrlich ascites carcinoma (EAC) cells with spectral and time-resolved fluorescence microscopy.

2. Experiment

2.1. Starting materials

Triethylphosphine oxide (TOPO), *L*- or *D*-cysteine (*L*- or *D*-Cys, respectively) hydrochloride and Trypan blue were purchased from Sigma-Aldrich and used without further purification. All biological reagents and materials were purchased from Biotot (Russia).

2.2. Preparation of the chiroptically active QDs

Chiroptical water-soluble QDs were prepared using the post-synthesis ligand exchange method using *L*- or *D*-cysteine as chiral ligands [16, 24]. A solution of *L*- or *D*-cysteine hydrochloride in methanol (0.2 mol l^{-1}) was added to a chloroform solution of CdSe/ZnS/TOPO-QDs (0.05 mmol l^{-1}) synthesized according to [25]. The volume of added solution did not exceed 10% of the initial volume of QD solution. The reaction mixture was shaken for 1 min and then water (pH 10, adjusted by 1 mol l^{-1} NaOH solution) was added. After 3–5 min the cysteine-capped CdSe/ZnS QDs transferred to the upper aqueous phase leaving the water-insoluble CdSe/ZnS/TOPO-QDs in the chloroform. Finally, the cysteine-capped CdSe/ZnS QDs were purified 3 times using 10 kDa Amicon Ultra centrifugal filter units. A comparison of FTIR spectra of TOPO-QDs and *L*-Cys QDs (see figure A1 in appendix A) shows the presence of cysteine characteristic bands and absence of TOPO bands in the FTIR spectrum of *L*-Cys QDs, which provides evidence for TOPO-to-cysteine ligand exchange.

2.3. Optical characterization

The UV/Vis absorption and fluorescence spectra were recorded using a UV-Probe 3600 spectrophotometer (Shimadzu) and a Cary Eclipse spectrofluorometer (Varian). Circular dichroism (CD) spectra of the *L*- or *D*-Cys QDs were recorded using a JASCO J-1500 (JASCO) spectrometer. A

Tensor 27 (Bruker) spectrometer was used for the FTIR analysis of the samples. The fluorescence quantum yields of the QD solutions were measured by the comparative method using Rhodamine 6G in ethanol as reference.

2.4. Cell culture

The Ehrlich ascites carcinoma (EAC) cell culture was obtained from the Petrov Research Institute of Oncology from white laboratory mice with an average weight of 20 g after 8–9 days of ascite growth. The mice were killed by cervical dislocation. The cell suspension was purified from the erythrocytes by 5 min treatment with a lysis buffer ($0.01 \text{ mol tris HCl}$, 0.87% NH_4Cl , pH = 7.4). The cells were then washed twice with Hank's Balanced Salt Solution (HBSS) and resuspended in RPMI-1640 medium with 10% of bovine embryonic serum and 100 U ml^{-1} penicillin.

2.5. Cell viability assay

For the cell viability estimation, the EAC cells were incubated with QDs in 6-well plates (ThermoFisher, USA) at 37°C in a humidified 5% CO_2 atmosphere for 24 h in RPMI-1640 containing 10% of bovine embryonic serum and 100 U ml^{-1} penicillin. The cell concentration was 4×10^6 cells per well. QD concentrations were 1, 4, 7, 10 and $20 \mu\text{mol l}^{-1}$. After the treatment procedure, viability of cells was evaluated by the Trypan blue test.

2.6. Confocal imaging of living cells

Incubation of EAC cells with QDs was carried out in 6-well plates (ThermoFisher, USA) in RPMI-1640 medium containing 10% of bovine embryonic serum and 100 U ml^{-1} penicillin at 37°C , 5% CO_2 , 90% relative humidity for 3, 6, 24, 48 and 96 h. QD concentration was $1 \mu\text{mol l}^{-1}$. Cell density was $1.2 \times 10^3/\text{mm}^2$. The viability of cells was more than 95% during the whole experiment. After incubation the cells were washed 3 times and suspended in HBSS. Confocal images of living cells were recorded with a LSM 710 (Zeiss) laser scanning confocal microscope equipped with a x20/0.4NA objective. QDs were excited with a diode laser 405 nm line. The emission was collected in the spectral region 500–560 nm corresponding to the QD emission band of 530 nm. The mean fluorescence signal per cell was quantitatively estimated using 'ImageJ' software (Wayne Rasband). Five independent measurements were performed after which the average fluorescence signal per cell and the respective standard deviations (SDs) were calculated by selecting 100 cells randomly observed on the fluorescence images.

Fluorescence spectra of *L*- or *D*-Cys QDs in living cells were obtained using standard operation modes of the LSM 710, which allows collection of the emission from the region of interest within the sample.

2.7. Fluorescence lifetime imaging

Fluorescence lifetime imaging was performed using a time-correlated single photon counting (TCSPC) spectrometer

(PicoQuant, Inc.) equipped with a $\times 40/0.65\text{NA}$ objective. A pulse laser radiation (405 nm) with an average power of 1 mW, pulse duration of 70 ps and repetition rate of 40 MHz was used for fluorescence excitation. A 500–560 nm bandpass filter was used to collect the QD emission. The measurements of fluorescence lifetime for *D*-Cys, *L*-Cys and TOPO-QD solutions were made with the QD concentration of $0.5 \mu\text{mol l}^{-1}$. Prior to obtaining fluorescence lifetime images of EAC cells with QDs, the EAC cells were incubated with *D*-Cys or *L*-Cys QDs for 3, 6, 24, 48 and 96 h under the previously described conditions. The concentration of QDs was equal to $10 \mu\text{mol l}^{-1}$. The following protocol was used for image acquisition. Cells were washed 3 times, suspended in HBSS and loaded into the glass hemocytometer. Data acquisition was performed from a $75 \times 75 \mu\text{m}^2$ area with a 512×512 pixel spatial resolution with a collection time of 5 ms per pixel. Parameters were chosen so that unlabeled cell autofluorescence did not yield a measurable signal. All experiments performed with EAC cells were carried out under the same instrumental settings.

The fluorescence lifetime image presents a 512×512 pixel 2D matrix with a measured FL lifetime value at each pixel. The QD FL lifetime was found to be well fitted by a multi-exponential decay model:

$$I(t) = \sum_n A_n \exp(-t/\tau_n) \quad (1)$$

where A_n are the amplitudes and τ_n are the fluorescent lifetimes. The fitting procedure was performed using the SymPhoTime 64 software (PicoQuant, Inc.).

Average lifetimes $\langle \tau \rangle$ were determined as the average time for which the emitters (QDs) remain in their excited state after the onset of excitation:

$$\langle \tau \rangle = \frac{\sum_n A_n \cdot \tau_n^2}{\sum_n A_n \cdot \tau_n} \quad (2)$$

3. Results and discussion

3.1. Chiroptically active QDs

The UV–Vis absorption and fluorescence spectra of trioctylphosphine oxide-capped CdSe/ZnS QDs (TOPO-QDs) and *D*- and *L*-cysteine capped CdSe/ZnS QDs (*D*- and *L*-Cys QDs, respectively) are presented in figure 1(A). The position of the first exciton absorption band of the TOPO-QDs corresponds to 512 nm, from which the diameter of the QDs was calculated analogously to the procedure described by Yu *et al* [26] and found to be approximately 2.5 nm.

It is reported [13–15] that chiral QDs produced from colloidal synthesis in the presence of chiral ligands generally do not exhibit exciton fluorescence, but demonstrate a broad fluorescence band instead, associated with surface defect states producing low luminescent quantum yields. On the contrary, in the post-synthesis phase transfer method used in

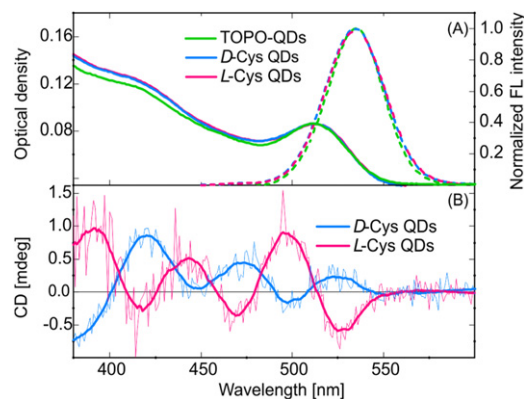


Figure 1. UV–Vis absorption (solid lines) and normalized fluorescence (lines and scatters) spectra (A) of TOPO-QDs in chloroform (green lines) and *D*- and *L*-Cys QDs in aqueous solution (blue and red lines) and circular dichroism spectra (B) of *D*- and *L*-Cys QDs in aqueous solution (blue and red lines). The concentrations of QDs C_{QD} were $0.2 \mu\text{mol l}^{-1}$ in (A) and $10 \mu\text{mol l}^{-1}$ in (B).

this work, chiral nanocrystals with intense exciton fluorescence have been formed. The *D*- and *L*-Cys QDs' intense exciton fluorescence at 530 nm is shown in figure 1(A) (dashed curves). No spectral signatures associated with QD aggregation such as a red shift or broadening of the fluorescence band were observed. However, an appreciable quenching of QD fluorescence occurred, which is probably due to the formation of additional defect states on the QD surface [27, 28].

The circular dichroism (CD) spectra of the *D*- and *L*-Cys QDs (figure 1(B)) show a pronounced opposite optical dichroism signal in the spectral region of the intrinsic QD absorption transitions (350–520 nm) while the TOPO-QDs show no CD signals (data not shown). The FTIR spectrum of *L*-Cys QDs, presented in figure A1 in appendix A, together with the CD spectra of the *D*- and *L*-Cys QDs provide evidence of TOPO-to-cysteine ligand exchange and the formation of the enantiomeric *D*- and *L*-forms of chiral QDs.

The fluorescence decay of the TOPO-QDs and *D*- and *L*-Cys QDs shows two relaxation processes with slow and fast characteristic times that are usually observed for colloidal solutions of the QDs at room temperature [28]. The slow decay process has a time constant τ_1 of tens of ns while the fast process shows a lifetime τ_2 of a few ns, as can be seen in table 1.

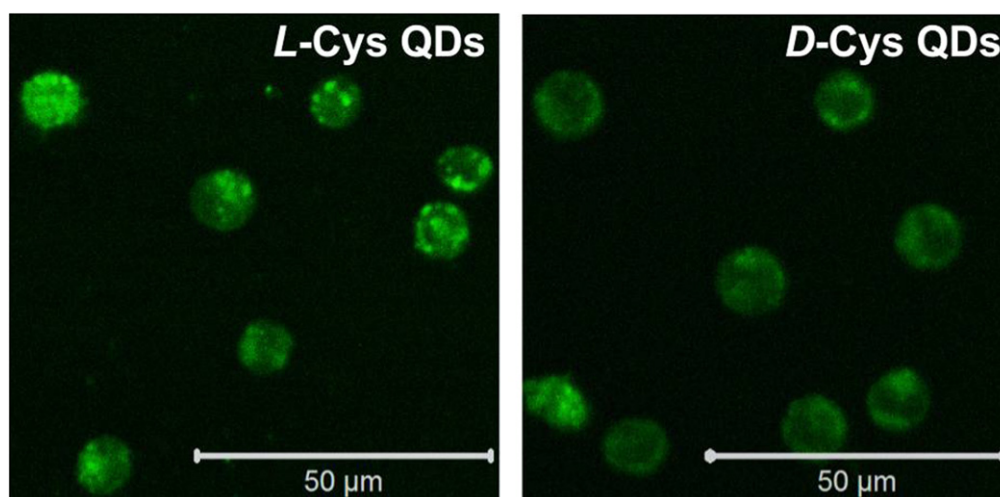
A comparative analysis of fluorescent properties of the *D*- and *L*-Cys QDs has shown that their fluorescence quantum yields and lifetimes are practically the same in aqueous solution (table 1).

3.2. In vitro biological testing of chiral QDs

Chiral *D*- and *L*-Cys QDs were used in *in-vitro* experiments in living EAC cells for which initial cytotoxicity tests demonstrated the absence of noticeable cytotoxicity in the $1\text{--}20 \mu\text{mol l}^{-1}$ range of QD concentrations (full data are shown in figure B1 in appendix B).

Table 1. Fluorescence characteristics of TOPO-capped and cysteine-capped CdSe/ZnS QDs.

Sample	Medium	FL quantum yield, φ [%]	$\tau_1/\tau_2/\tau_3$ [ns]	$\langle\tau\rangle$ [ns]
TOPO-QDs	<i>chloroform solution</i>	11.6	20/5/-	18.0
<i>L-Cys</i> QDs	<i>aqueous solution</i>	5	14/4/-	10.5
	<i>RPMI-1640 (with bovine embryonic serum)</i>	7.5	19/3/-	13.0
<i>D-Cys</i> QDs	<i>EAC cells</i>	—	20/9/3	15.0
	<i>aqueous solution</i>	5	14/4/-	10.5
	<i>RPMI-1640 (with bovine embryonic serum)</i>	7.5	19/3/-	13.0
	<i>EAC cells</i>	—	21/10/4	16.0

**Figure 2.** Fluorescent images of EAC cells incubated with *D*- and *L*-Cys QDs after 96 h of incubation. QD concentration in the incubation medium is $2 \mu\text{mol l}^{-1}$.

The degree of aggregation in the quantum dot solutions is critical for cellular uptake. The medium (RPMI-1640) that we used contains only homochiral *L*- amino acids. Therefore, enantioselective QD aggregation could take place there, and it could lead to a difference in intracellular concentration of *D*- and *L*-Cys QDs. To explore the possible enantioselective aggregation of chiral QDs in the incubation medium we had carefully examined the spectral-luminescent properties of the *D*- and *L*-Cys QDs. It was observed that *D*- and *L*-Cys QDs in the incubation medium have practically the same FL quantum yields and lifetimes, as can be seen in table 1. Therefore, no evidence of enantioselective QD aggregation (for details see appendix C) was observed.

In order to study the chiral dot cellular uptake several samples of cells incubated with *D*- or *L*-Cys QDs during different time periods were prepared. Fluorescent intensity of the chiral QDs in EAC cells was assessed by analysis of the fluorescence images obtained after 3, 6, 24, 48 and 96 h of incubation with QDs at $2 \mu\text{mol l}^{-1}$ concentration.

The fluorescence images of the cells after 96 h of incubation with QDs presented in figure 2 clearly confirm the intracellular uptake and accumulation of the chiral QDs into the cells, showing their characteristic fluorescent labeling. The bright fluorescence spots observed within the cells reflect the intracellular distribution of QDs due to, most likely, their endosomal-like localization.

Fluorescence spectra of chiral QDs in the cells are presented in figure 3(A). It can be seen that the localization of QDs in vesicles leads to a red shift of the QD fluorescence band with respect to its position in aqueous solution. This may be caused by dot-to-dot energy transfer in cell vesicles where relatively high local QD concentrations are achieved [23]. However, the fluorescence band positions and bandwidths of *D*- and *L*-Cys QDs in the vesicles are practically the same, indicating an absence of enantioselective effects on their FL spectra.

The mean fluorescence intensity per cell increases with incubation time (3, 6, 24, 48 and 96 h) for both QD enantiomeric forms as is shown in figure 3(B). Moreover, the intensity of the fluorescence of *L*-Cys QDs is higher than that of *D*-Cys QDs for any incubation time and becomes twice as intense after 96 h.

FLIM images of EAC cells, incubated with *D*- and *L*-Cys QDs for 24 h, presented in figure 4 show bright spots corresponding to QDs inside the vesicles.

As shown in figure 4, the fluorescence decays associated with the intracellular CdSe/ZnS QDs are significantly longer than those of CdSe/ZnS QDs in aqueous solution, and three-exponential functions (table 1) describe better the CdSe/ZnS QD fluorescence decay in vesicles. Analogous data were obtained for other incubation times. The increase of the fluorescence lifetime and the appearance of the third component in the fluorescence decays together with the red shift of

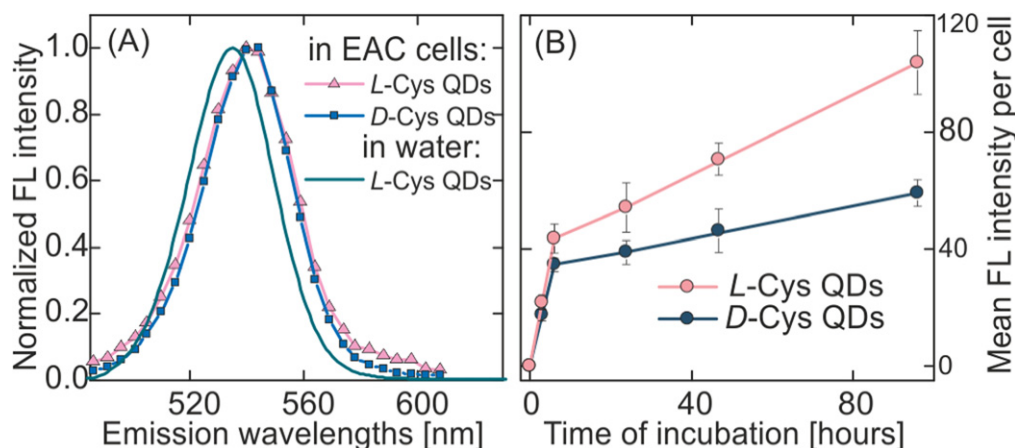


Figure 3. Fluorescence spectra of *D*- and *L*-Cys QDs in cells and in water (A). Intracellular fluorescence intensity per cell for *D*- and *L*-Cys QDs versus incubation time (B). The QD concentration in incubation medium is $1 \mu\text{mol l}^{-1}$. Error bars in (B) are the SD of five different experiments.

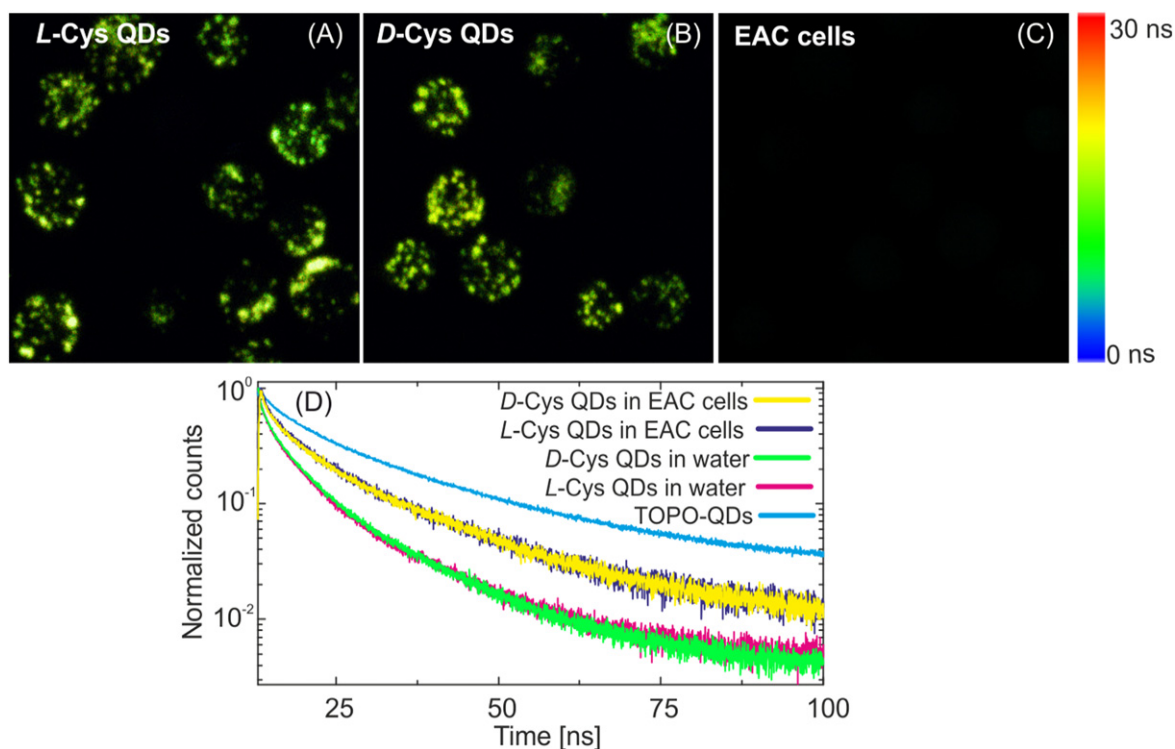


Figure 4. FLIM images of EAC cells incubated with *L*-Cys QDs (A) and *D*-Cys QDs (B) after 24 h of incubation. The QD concentration in the incubation medium is $1 \mu\text{mol l}^{-1}$. (C) FLIM image of the EAC cells. (D) Fluorescence decay curves for TOPO-QDs in chloroform solution, as well as for *D*- and *L*-Cys QDs in aqueous solution and in the EAC cells.

the intracellular fluorescence band (figure 3(B)) are a sign of dot-to-dot energy transfer [29] in the vesicles. However, it is important to note that the fluorescence lifetimes of *D*- and *L*-Cys QDs in the vesicles are practically the same (see also table 1) for all incubation times used. This fact indicates the absence of enantioselective fluorescence quenching upon QD incorporation into the cells and enables the use of fluorescence intensity to estimate the chiral CdSe/ZnS QD relative concentration inside the cells. Therefore, the more intensive fluorescence of the *L*-Cys QDs, as compared with that of the

D-Cys QDs, clearly shows that a higher concentration of *L*-Cys QDs is due to more efficient cellular uptake.

4. Conclusions

The influence of the chirality of CdSe/ZnS quantum dots on their cellular uptake has been investigated using living EAC cells by spectral and time-resolved fluorescence microscopy. Comparative analysis of the fluorescence intensities and

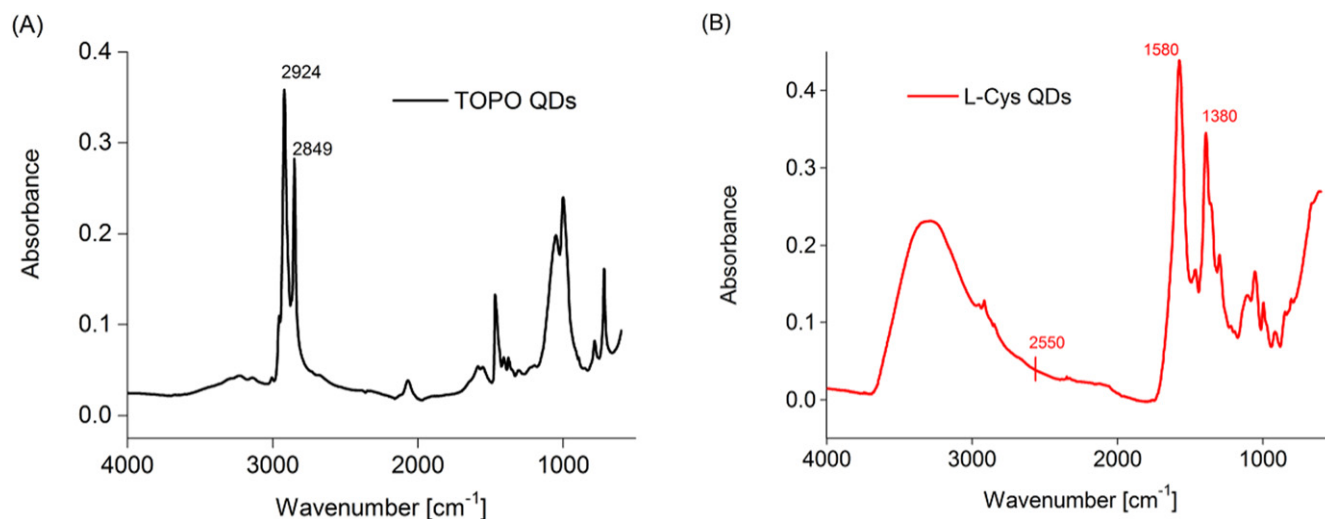


Figure A1. FTIR spectra of TOPO-QDs (A) and *L*-Cys QDs (B).

lifetimes of *L*-Cys and *D*-Cys QDs in the cells shows enantioselective cellular uptake of chiral QDs, namely that *L*-Cys QD uptake is almost twice that of *D*-Cys QDs. We believe that this finding may lay the groundwork for novel approaches to controlling the biological properties and behavior of man-made chiral nanomaterials in living cells.

This work was supported by the Ministry of Education and Science of the Russian Federation (Projects 14. B25.31.0002, 3.109.2014/K and Grant 074-U01 through ITMO Post-Doctoral Fellowship) and Science Foundation Ireland (project SFI 12/IA/1300).

Appendix A

A.1. FTIR

The FTIR spectrum of the TOPO-QDs (figure A1(A)) is dominated by characteristic bands of TOPO at 2849 and 2924 cm⁻¹ that reveal the presence of TOPO on the QD surface [30]. In the spectrum of *L*-cysteine-capped CdSe/ZnS QDs (figure A1(B)), the bands of TOPO disappeared and several peaks characteristic for cysteine appear to be: at 1380 cm⁻¹ corresponding to the symmetric stretching vibration of the COO⁻ group; and at 1580 cm⁻¹ corresponding to the asymmetric bending vibration of the NH₃⁺ group [31]. The presence of the two peaks in the region around 1380 and 1580 cm⁻¹ confirms that these groups are free [32]. The absence of a peak at 2550 cm⁻¹ corresponding to the -SH group in free cysteine indicates that the cysteine molecules are bound to the QD surface via this group.

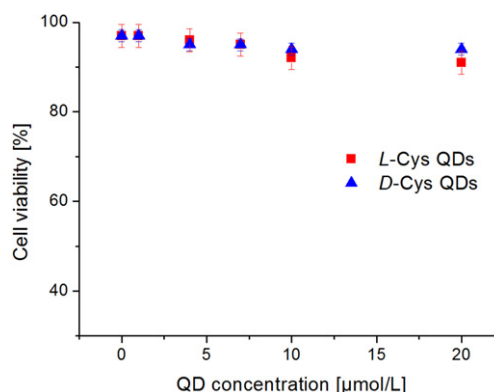


Figure B1. EAC cell viability data after incubation with chiral QDs for 24 h, represented as the percentage of viable cells obtained from the Trypan blue assay of EAC cells.

Appendix B

B.1. Cell viability assay

It is well known from previous studies that CdSe/ZnS core-shell QDs have sufficiently low cytotoxicity as compared with CdSe QDs without a shell [33, 34]. In our experiment, cell death rate also did not exceed 10% in the concentration region 1–20 μmol L⁻¹ of QDs (see figure B1). *L*-Cys QDs had slightly higher cytotoxicity than *D*-Cys QDs. Similar results were obtained in the previous work [18].

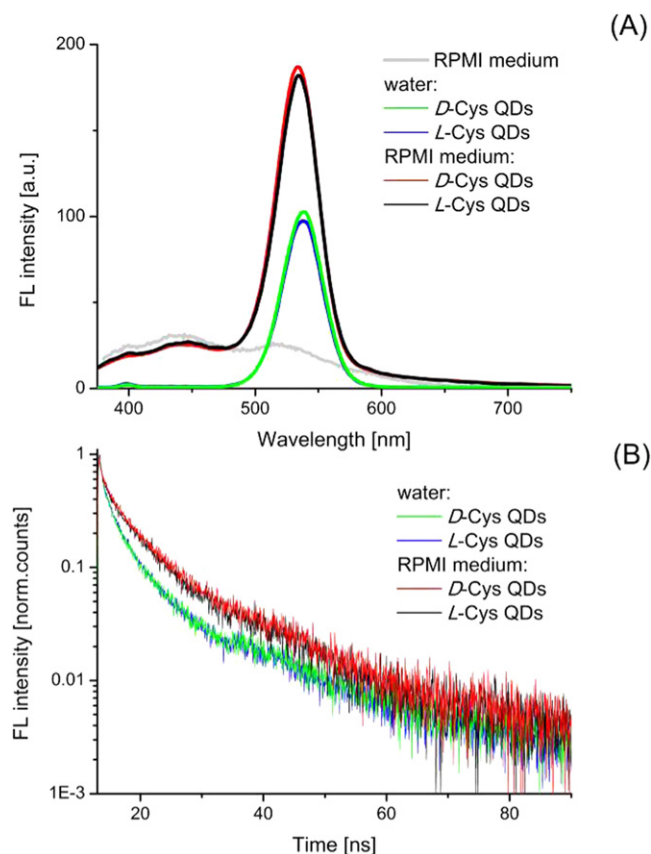


Figure C1. Fluorescence spectra (A) and fluorescence decay curves (B) of *L*- and *D*-Cys CdSe/ZnS QDs with identical concentration ($1 \mu\text{mol l}^{-1}$) in water and in RPMI-1640 medium containing 10% of bovine serum. The excitation wavelength is 350 nm.

Appendix C

C.1. Fluorescence properties of *L*- and *D*-Cys QDs in the incubation medium

The cell incubation with QDs was performed in RPMI-1640 medium containing 10% of bovine serum. This medium consists of only *L*-amino acids, which potentially may influence the aggregation of *D*-Cys QDs and consequently hamper their cellular uptake. In order to examine a possible enantioselective aggregation of chiral QDs in the incubation medium we have compared the fluorescence properties of *L*- and *D*-Cys QDs in RPMI-1640 with 10% of serum and in water. Analysis of fluorescence spectra (figure C1(A)) reveals no difference in the intensity and spectral position of the fluorescence bands for both *L*- and *D*-Cys QDs in the medium. The FL quantum yield of *L*- and *D*-Cys QDs was also the same in the medium, and was noticeably increased compared with that in water. The increase in the fluorescence quantum yield of QDs observed in the medium can be explained by the passivation of the QD surface with proteins and other biocompounds [35].

(A) In order to visualize possible QD aggregation in water and in the incubation medium, we analyzed QD fluorescence lifetimes. Fluorescence decay curves of *L*- and *D*-Cys QDs in water and in RPMI-1640 medium containing 10% of bovine serum are presented in figure C1(B). As can be seen, the fluorescence decays of *L*- and *D*-Cys QDs in the incubation medium are practically identical to each other. Thus, *L*- and *D*-Cys QDs do not demonstrate any evidence of enantioselective aggregation in the incubation medium, which can have an effect on intracellular concentration of chiral QDs.

References

- (B)
- [1] Cintas P 2002 Chirality of living systems: a helping hand from crystals and oligopeptides *Angew. Chem., Int. Ed. Engl.* **41** 1139–45
 - [2] Yan W, Xu L, Xu C, Ma W, Kuang H, Wang L and Kotov N A 2012 Self-assembly of chiral nanoparticle pyramids with strong R/S optical activity *J. Am. Chem. Soc.* **134** 15114–21
 - [3] Govan J E, Jan E, Querejeta A, Kotov N A and Gun'ko Y K 2010 Chiral luminescent CdS nano-tetrapods *Chem. Commun.* **46** 6072–4
 - [4] Zhao Y, Xu L, Ma W, Wang L, Kuang H, Xu C and Kotov N A 2014 Shell-engineered chiroplasmonic assemblies of nanoparticles for zeptomolar DNA detection *Nano Lett.* **14** 3908–13
 - [5] Xia Y, Zhou Y and Tang Z 2011 Chiral inorganic nanoparticles: origin, optical properties and bioapplications *Nanoscale* **3** 1374–82
 - [6] Efros A L, Lockwood D J and Tsybeskov L 2003 *Semiconductor Nanocrystals: From Basic Principles to Applications* (New York: Springer)
 - [7] Medintz I L, Uyeda H T, Goldman E R and Mattoussi H 2005 Quantum dot bioconjugates for imaging, labelling and sensing *Nat. Mater.* **4** 435–46
 - [8] Maslov V, Orlova A and Baranov A 2012 *Photosensitizers in Medicine, Environment, and Security* (New York, USA: Springer) p 351
 - [9] Li L, Zhao J F, Won N, Jin H, Kim S and Chen J Y 2012 Quantum dot-aluminum phthalocyanine conjugates perform photodynamic reactions to kill cancer cells via fluorescence resonance energy transfer *Nanoscale Res. Lett.* **7** 386
 - [10] Martynenko I V, Orlova A O, Maslov V G, Baranov A V, Fedorov A V and Artemyev M 2013 Energy transfer in complexes of water-soluble quantum dots and chlorin e6 molecules in different environments *Beilstein J. Nanotechnol.* **4** 895–902
 - [11] Martynenko I V *et al* 2015 Chlorin e6–ZnSe/ZnS quantum dots based system as reagent for photodynamic therapy *Nanotechnology* **26** 055102
 - [12] Zhou Y, Yang M, Sun K, Tang Z and Kotov N A 2010 Similar topological origin of chiral centers in organic and nanoscale inorganic structures: effect of stabilizer chirality on optical isomerism and growth of CdTe nanocrystals *J. Am. Chem. Soc.* **132** 6006–13
 - [13] Moloney M P, Gun'ko Y K and Kelly J M 2007 Chiral highly luminescent CdS quantum dots *Chem. Commun.* 3900–2
 - [14] Elliott S D, Moloney M P and Gun'ko Y K 2008 Chiral shells and achiral cores in CdS quantum dots *Nano Lett.* **8** 2452–7
 - [15] Ben Moshe A, Szwarcman D and Markovich G 2011 Size dependence of chiroptical activity in colloidal quantum dots *ACS Nano* **5** 9034–43
 - [16] Tohgha U, Varga K and Balaz M 2013 Achiral CdSe quantum dots exhibit optical activity in the visible region upon post-

- synthetic ligand exchange with d- or l-cysteine *Chem. Commun.* **49** 1844–6
- [17] Mukhina M V, Maslov V G, Baranov A V, Fedorov A V, Orlova A O, Purcell-Milton F, Govan J and Gun'ko Y K 2015 Intrinsic chirality of CdSe/ZnS quantum dots and quantum rods *Nano Lett.* **15** 2844–51
- [18] Li Y, Zhou Y, Wang H-Y, Perrett S, Zhao Y, Tang Z and Nie G 2011 Chirality of glutathione surface coating affects the cytotoxicity of quantum dots *Angew. Chem., Int. Ed.* **50** 5860–4
- [19] Soenen S J, Demeester J, De Smedt S C and Braeckmans K 2012 The cytotoxic effects of polymer-coated quantum dots and restrictions for live cell applications *Biomaterials* **33** 4882–8
- [20] Carlini L and Nadeau J L 2013 Uptake and processing of semiconductor quantum dots in living cells studied by fluorescence lifetime imaging microscopy (FLIM) *Chem. Commun.* **49** 1714–6
- [21] Conroy J, Byrne S J, Gun'ko Y K, Rakovich Y P, Donegan J F, Davies A, Kelleher D and Volkov Y 2008 CdTe nanoparticles display tropism to core histones and histone-rich cell organelles *Small* **4** 2006–15
- [22] Orte A, Alvarez-Pez J M and Ruedas-Rama M J 2013 Fluorescence lifetime imaging microscopy for the detection of intracellular pH with quantum dot nanosensors *ACS Nano* **7** 6387–95
- [23] Dong C Q, Chowdhury B and Irudayaraj J 2013 Probing site-exclusive binding of aqueous QDs and their organelle-dependent dynamics in live cells by single molecule spectroscopy *Analyst* **138** 2871–6
- [24] Zhou Y, Zhu Z, Huang W, Liu W, Wu S, Liu X, Gao Y, Zhang W and Tang Z 2011 Optical coupling between chiral biomolecules and semiconductor nanoparticles: size-dependent circular dichroism absorption *Angew. Chem., Int. Ed.* **50** 11456–9
- [25] Talapin D V, Rogach A L, Kornowski A, Haase M and Weller H 2001 Highly luminescent monodisperse CdSe and CdSe/ZnS nanocrystals synthesized in a hexadecylamine–trioctylphosphine oxide–trioctylphosphine mixture *Nano Lett.* **1** 207–11
- [26] Yu W W, Qu L, Guo W and Peng X 2003 Experimental determination of the extinction coefficient of CdTe, CdSe, and CdS nanocrystals *Chem. Mater.* **15** 2854–60
- [27] Baker D R and Kamat P V 2010 Tuning the emission of CdSe quantum dots by controlled trap enhancement *Langmuir* **26** 11272–6
- [28] Peterson M D, Cass L C, Harris R D, Edme K, Sung K and Weiss E A 2014 The role of ligands in determining the exciton relaxation dynamics in semiconductor quantum dots *Annu. Rev. Phys. Chem.* **65** 317–39
- [29] Kruchinin S Y, Fedorov A V, Baranov A V, Perova T S and Berwick K 2008 Resonant energy transfer in quantum dots: frequency-domain luminescent spectroscopy *Phys. Rev. B* **78** 125311
- [30] Shi Y, He P and Zhu X 2008 Photoluminescence-enhanced biocompatible quantum dots by phospholipid functionalization *Mater. Res. Bull.* **43** 2626–35
- [31] Pawlukoć A, Leciejewicz J, Ramirez-Cuesta A J and Nowicka-Scheibe J 2005 l-cysteine: neutron spectroscopy, Raman, IR and *ab initio* study *Spectrochim. Acta A* **61** 2474–81
- [32] Baláž M, Baláž P, Tjuliev G, Zubřík A, Sayagués M, Zorkovská A and Kostova N 2013 Cystine-capped CdSe@ZnS nanocomposites: mechanochemical synthesis, properties, and the role of capping agent *J. Mater. Sci.* **48** 2424–32
- [33] Peng L, He M, Chen B, Wu Q, Zhang Z, Pang D, Zhu Y and Hu B 2013 Cellular uptake, elimination and toxicity of CdSe/ZnS quantum dots in HepG2 cells *Biomaterials* **34** 9545–58
- [34] Brunetti V, Chibli H, Fiammengio R, Galeone A, Malvindi M A, Vecchio G, Cingolani R, Nadeau J L and Pompa P P 2013 InP/ZnS as a safer alternative to CdSe/ZnS core/shell quantum dots: *in vitro* and *in vivo* toxicity assessment *Nanoscale* **5** 307–17
- [35] Amelia M, Flamini R and Latterini L 2010 Recovery of CdS nanocrystal defects through conjugation with proteins *Langmuir* **26** 10129–34